Research on Chemical Intermediates (2020) 46:2481–2496
https://doi.org/10.1007/s11164-020-04102-1

Methane activation at low temperature in an acidic electrolyte using PdAu/C, PdCu/C, and $PdTiO_2$/C electrocatalysts for PEMFC

Felipe de Moura Souza[2] · Rodrigo Fernando Brambilla de Souza[1] · Bruno Lemos Batista[2] · Mauro Coelho dos Santos[2] · Fabio Coral Fonseca[1] · Almir Oliveira Neto[1] · Julio Nandenha[1]

Received: 18 November 2019 / Accepted: 8 February 2020 / Published online: 12 March 2020

Abstract

Pd/C, PdAu/C, PdCu/C, and $PdTiO_2$/C electrocatalysts were prepared by a sodium borohydride reduction process for methane activation at low temperatures in a PEMFC reactor. These electrocatalysts were characterized by XRD, TEM, XPS, ICP-MS, ATR-FTIR, and cyclic voltammetry. The diffractograms of Pd/C, PdAu(50:50)/C, PdCu(50:50)/C, and $PdTiO_2$(50:50)/C electrocatalysts showed peaks associated with Pd face-centered cubic structure. PdAu(50:50)/C showed a small shift in the peak center when it was compared to Pd/C, while PdCu(50:50)/C showed a shift to higher angles when it was also compared to Pd/C. This effect can be due to the formation of an alloy between Pd and Au, and Pd and Cu. By TEM experiments, a mean nanoparticle size was observed between 6.9 and 8.9 nm for all electrocatalysts. Cyclic voltammograms of Pd/C, PdAu/C, PdCu/C and $PdTiO_2$/C electrocatalysts showed an increase in current density values after the adsorption of methane The ATR-FTIR experiments showed for all electrocatalysts the formation of methanol and formic acidic. Polarization curves at 80 °C acquired in a PEMFC reactor showed that PdAu(50:50)/C and $PdTiO_2$(50:50)/C had superior performance when compared to Pd/C, indicating the beneficial effect of adding the co-catalyst; this behavior has been attributed to the bifunctional mechanism or electronic effect.

Keywords Sodium borohydride reduction process · Pd binary electrocatalysts · Methane oxidation · PEMFC reactor · ATR-FTIR studies

✉ Julio Nandenha
nandenhajb@yahoo.com.br

[1] Instituto de Pesquisas Energéticas e Nucleares, IPEN/CNEN-SP, Av. Prof. Lineu Prestes, 2242 Cidade Universitária, Sãopaulo, SP CEP 05508-000, Brazil

[2] Centro de Ciências Naturais e Humanas, Universidade Federal do ABC, Rua Santa Adélia, 166, Santo André, SP 09210-170, Brazil

Introduction

The recent advances in drilling technologies facilitated access to natural gas. Therefore, it reduced the expenses of the production process [1–3]. However, this compost could be considered an efficient alternative fuel for low-emission transportation because it burns more cleanly with near-zero particulate matter [1]. The use of methane in the energy sector has been related to the combustion process. Therefore, a new alternative would be to use methane in a type of proton exchange membrane fuel cells (PEMFCs) reactor.

The fuel cell reactor type is a competitive alternative to provide energy considering a conversion of chemical into electrical energy by an electrochemical reaction with possible formation of products with higher value [4–6]. They consist of electrodes at the anode (negative), cathode (positive), and a membrane (electrolyte) interspersed between the electrodes [6, 7]. These PEMFC fuel cells have high efficiencies, flexibility in size, low sound emission operation, and almost zero emissions of pollutants [7–9].

Platinum and palladium electrocatalysts have been proposed for methane oxidation at room temperature [1, 6]. The Pt and Pd electrocatalysts are also efficient for the combustion of hydrocarbons and CO [10, 11]. Pd electrocatalysts have been considered better for methane combustion. In contrast, Pt electrocatalysts are better for the oxidation process regarding others hydrocarbons [12].

Recently, Joglekar et al. [9] developed a new electrocatalyst for electrochemical oxidation of methane in a (PEMFC) at 80 °C. In this work, a maximum standard power of 403 μW mg^{-1} was obtained, which is five times higher than the power energy obtained from a commercial electrocatalyst and two orders of magnitude higher than from a Pt carbon black.

Sekizawa et al. [13, 14] investigated Pd electrocatalysts for the methane oxidation at low temperature. All Pd/ZrO_2 and Pd/SnO_2 electrocatalysts showed high activity despite their small surface areas. For Pd/ZrO_2, the electrochemical activity was considered dependent on the crystalline phase. According to these authors, a monoclinic phase of ZrO_2 increased the activity in comparison with the tetragonal phase. For Pd/SnO_2, the impregnation of Pd on SnO_2 solution was the most effective using $Pd(C_5H_7OO)_2$ [13].

The addition of oxides such as CeO_2, RuO_2, SnO_2, TiO_2, WO_3, and V_2O_5 to carbon as support [15, 16] has also increased the electrochemical activity regarding oxidation of small organic molecules by the synergistic interaction between oxides, carbon, and noble metals. The presence of metallic oxides favors the oxidation of some intermediates adsorbed on palladium or platinum.

Chang el al. [17] applied copper to reduce CO_2 to methanol by water activation, and Munoz et al. [18] indicated that PdCu/C was more efficient than Pd/C regarding ethylene glycol oxidation, propylene glycol, and glycerol in alkaline media. This effect was attributed to both bifunctional and electronic effect.

Assumpção et al. [19] showed that Pd/C-TiO_2 was promising toward ethanol oxidation in alkaline electrolytes, where these results were attributed to the

presence of carbon and TiO_2, where the TiO_2 supplies OH^-species and also changes the Pd d-band by a strong metal–support interaction.

Neto et al. [20] showed that PdAu/C was promising for formate oxidation in comparison with Pd/C, where the presence of Au in small quantities which contribute to the formate adsorption.

Agarwal et al. [21] showed that the oxidation of methane could be favored in PdAu(50:50)/TiO_2 electrocatalysts, where the methane was oxidized to methanol with high selectivity at mild temperatures. These authors concluded that H_2O_2 activates methane, which incorporates molecular oxygen through a radical process.

The aim of this work was to prepare Pd/C, PdAu/C, PdCu/C, and PdTiO_2/C by a sodium borohydride reduction method and apply them for electrochemical oxidation of methane in acidic medium.

Experimental

Electrocatalysts synthesis

20% Pd/C, 20% PdAu(50:50)/C, 20% PdCu(50:50)/C and 20% PdTiO_2(50:50)/C electrocatalysts were prepared using $Pd(NO_3)_2{\cdot}2H_2O$ (Aldrich) and $HAuCl_4{\cdot}3H_2O$ (Aldrich), $CuCl_2{\cdot}2H_2O$ (Sigma-Aldrich), and TiO_2 as metal sources and $NaBH_4$ was used as a reducing agent and Carbon XC72 was used as support [22–24]. The choice of the respective binary compositions was based on Agarwal et al. [21] works. The Vulcan Carbon XC72 was dispersed into a solution containing metal ions of Pd, Au, Cu, or TiO_2. This solution was dispersed to an Ultrason by 10 min for homogenization after the $NaBH_4$ solution was added. This solution now was maintained under stirring for an additional 1 h at room temperature for the reduction of the metal salts. After that, the resulting material was filtered, washed with ultrapure water, and dried in a thermostatic laboratory stove at 70 °C for 2 h [25–27]. Then, the electrocatalysts were macerated and a thin powder was obtained, and its mass was weighed on a semi-analytical scale to check the present metal load.

X-ray diffraction (XRD) and transmission electron microscopy (TEM)

Pd/C, PdAu/C, PdCu/C, and PdTiO_2/C electrocatalysts were characterized by X-ray diffraction analysis using a CuKα radiation source. The diffractograms were recorded according to the works [16, 28, 29]. The morphology and nanoparticle distribution of the electrocatalysts were determined by transmission electron microscopy using an electron microscope model JEM-2100. The construction of the histograms and determination of the mean nanoparticle sizes were measured over 170 nanoparticles from seven micrographs [20, 26].

Elemental composition by ICP-MS analysis

The ICP-MS analysis (Agilent 7900) was utilized to determine the elemental composition of electrocatalysts prepared. The Pd, Au, Ti, and Cu extraction was carried out using a closed vessel system. Approximately 20 mg of the electrocatalyst was placed into 50-mL test tubes that contained 3 mL of nitric acidic solution + 1 mL of hydrochloric acid. The isotopes monitored were ^{105}Pd, ^{63}Cu, ^{197}Au, and ^{47}Ti.

X-ray photoelectron spectroscopy (XPS)

XPS measurements were carried out using a Thermo Scientific K-Alpha^{+} spectrometer, monochromated with Al Kα X-ray source radiation ($h\nu = 1486.6$ eV) and a spot diameter of 400 µm at base pressure below 5×10^{-7} Pa. Peak energies were given to an accuracy of 0.1 eV, and peak areas were normalized by using appropriate atomic sensitivity factors. The spectra were deconvoluted and optimized using a Levenberg–Marquardt algorithm in the Casa XPS software.

Cyclic voltammetry (CV)

The cyclic voltammetry of electrocatalysts was carried out with AutoLab PGSTAT30 Potentiostat/Galvanostat with GPES software coupled to the interface, at 25 °C in a 0.5 mol L^{-1} H_2SO_4 solution using a three-electrode conventional cell [23]. The CV experiments were done at a scan rate of 10 mV s^{-1} according to reference [27].

Attenuated total reflection: Fourier transform infrared (ATR-FTIR)

The ATR-FTIR measurements were performed on a spectrometer equipped with an MCT detector cooled with liquid N_2. The ATR accessory with internal reflection element diamond/ZnSe is coupled to the spectrometer [30], where an electrochemical cell is connected above the internal reflection element. The working electrode was an ultrathin porous carbon coating technique in the presence of CH_4 gas saturated in 0.5 mol L^{-1} H_2SO_4 for 1.800 s. The background spectra were collected following Nandenha et al. work [27].

Fuel cell experiment

For experiments in fuel cell, the membrane electrode assemblies (MEAs) were prepared by hot pressing at 125 °C for 5 min under pressure of 225 kgf cm^{-2} using a pretreated Nafion® 117 membranes placed between anode (Pd/C, PdAu/C, PdCuC, and $PdTiO_2$/C) and cathode with Pt/C BASF electrocatalysts. The binaries anode electrodes and the cathode prepared were made with 1 mg Pd cm^{-2} electrocatalyst loading [19, 25]. The methane studies were realized in accordance with reference

27. Polarization curves were obtained using AutoLab PGSTAT302N with GPES software coupled, which receives the electric current produced by, and connected in the fuel cell.

Results and discussion

The X-ray diffractograms of the Pd/C, PdAu/C, PdCu/C, and $PdTiO_2$/C electrocatalysts synthesized by the sodium borohydride are shown in Fig. 1. Pd/C, PdAu/C, PdCu/C, and $PdTiO_2$/C electrocatalysts showed a broad peak centered at approximately $2\theta = 25^{o}$; this peak was associated with the (002) plane of the carbon support material. All electrocatalysts also presented peaks at about $2\theta = 40°$, 46°, 67° and 81° associated with the planes (111), (200), (220) and (311) of Pd face-centered cubic structure (JCPDS # 46-1043). $PdTiO_2C$ showed peaks at approximately $2\theta = 25°$, 37°, 38°, 39°, 48°, 54°, 69° and 70° associated with the tetragonal structure (JCPDF Card # 2-387) characteristics of titanium oxide (TiO_2) anatase phase. PdAu/C electrocatalyst showed a shift to smaller angles compared to Pd/C, indicating the incorporation of Au into the Pd lattice, consequently forming Pd–Au alloys [22]. Assumpção et al. [19] showed diffractograms peaks of PtAu/C shifted to lower 2θ values when compared to Pt/C, and they also suggested the formation of PtAu alloy. PdCu/C electrocatalysts also showed a shift to larger angles compared to Pd/C, also indicating the formation of an alloy characterized by the insertion of Cu atoms in the crystalline structure of Pd. Ottoni et al. [31] showed that PtCu/C prepared by different compositions by a borohydride reduction process had diffraction peaks located in higher values of 2θ, so these authors concluded that the incorporation of Cu atoms in the platinum crystalline structure occurred.

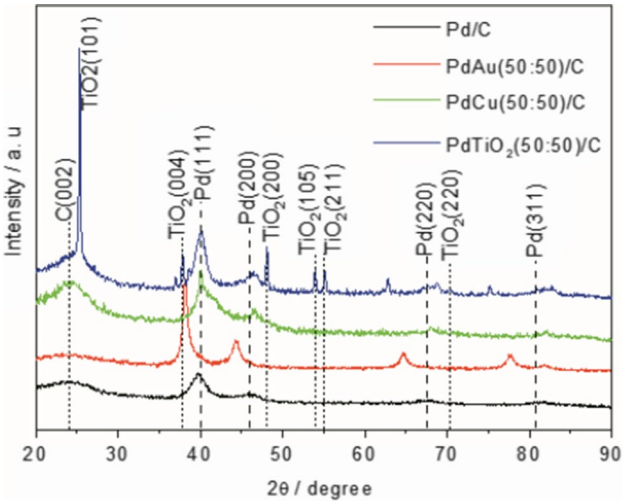

Fig. 1 X-ray diffractograms of the Pd/C, PdAu(50:50)/C, PdCu(50:50)/C, and $PdTiO_2$(50:50)/C electrocatalysts synthesized by the sodium borohydride reduction method

The micrographs and the nanoparticle size distribution of Pd/C, PdAu/C, PdCu/C, and $PdTiO_2$/C are shown in Fig. 2. The images obtained revealed that the nanoparticles were well dispersed in the support. However, $PdTiO_2$/C showed the presence of

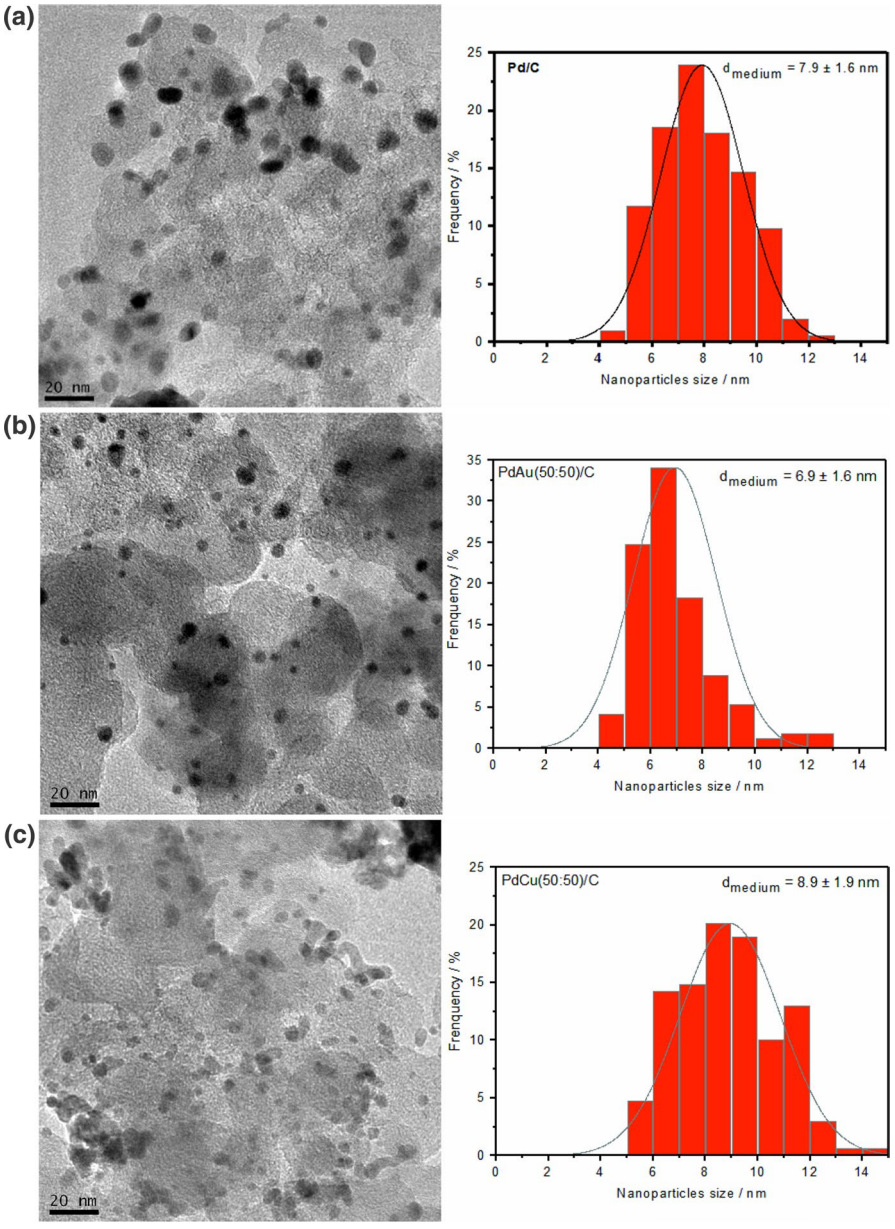

Fig. 2 TEM images and histograms of the nanoparticle size distribution to: **a** Pd/C, **b** PdAu(50:50)/C, **c** PdCu(50:50)/C, and **d** PdTiO2(50:50)/C electrocatalysts

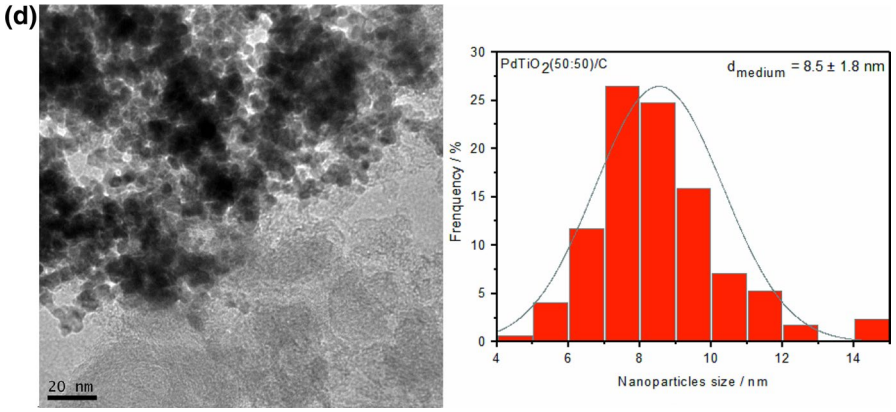

Fig. 2 (continued)

some agglomerates. The synthesized materials showed a mean nanoparticle size of 6.9–8.9 nm with deviations standard from 1.6 to 1.9 nm, respectively.

The results of ICP-MS showed that the amount of Pd in the synthesized electrocatalysts is close to that expected, according to Table 1. The obtained values of Pd by ICP-MS were used in the normalization of the electrocatalytic activity of the electrocatalysts in this work.

To further explore the chemical properties of the electrocatalysts, XPS analysis was performed. XPS survey scans identified and quantified the chemical species constituent of the electrocatalysts. As shown in Fig. 3, the atomic ratio of metals of the PdAu/C and $PdTiO_2$/C electrocatalysts is close to that expected, but the concentration of the PdCu(50:50)/C is lower because there is a low atomic concentration on the surface of this electrocatalyst.

XPS spectra were obtained to identify the oxidation states of metals in the near-surface region (< 3 nm) of the electrocatalysts with high resolution of Pd 3*d*, Ti 2*p*, Au 4*f*, and Cu 2*p*. As displayed in Fig. 4, the deconvoluted Pd 3d spectra exhibit a spin–orbit doublet with Pd $3d_{5/2}$ and Pd $3d_{3/2}$ at 335.2 and 340.5 eV to Pd^0, and 336.5 and 340.8 eV to Pd^{+2}, respectively, for Pd/C, as is reported in the literature [32–34]. We can see that all binary electrocatalysts showed positive shifts to Pd^0

Table 1 Pd, Au, Cu and TiO_2 mass ratio obtained by using ICP-MS and XPS

Electrocatalyst	Pd nominal (%)	Pd ICP-MS (%)	Pd XPS (%)	2nd metal nominal (%)	2nd metal ICP-MS (%)	2nd metal XPS (%)
Pd/C	20.0	18.2 ± 0.1	24.9	n.d.	n.d.	n.d.
PdAu(50:50)/C	7.0	6.8 ± 0.2	7.8 ± 0.6	13	14.7 ± 0,1	12.2 ± 1.0
PdCu(50:50)/C	12.5	13.3 ± 0.2	18.8 ± 1.5	7.5	8.9 ± 0.2	4.0 ± 1.7
$PdTiO_2$(50:50)/C	11.4	12.7 ± 0.1	9.7 ± 1.7	8.6	0.36 ± 0.2	1.7 ± 1.4

n.d. = not determined

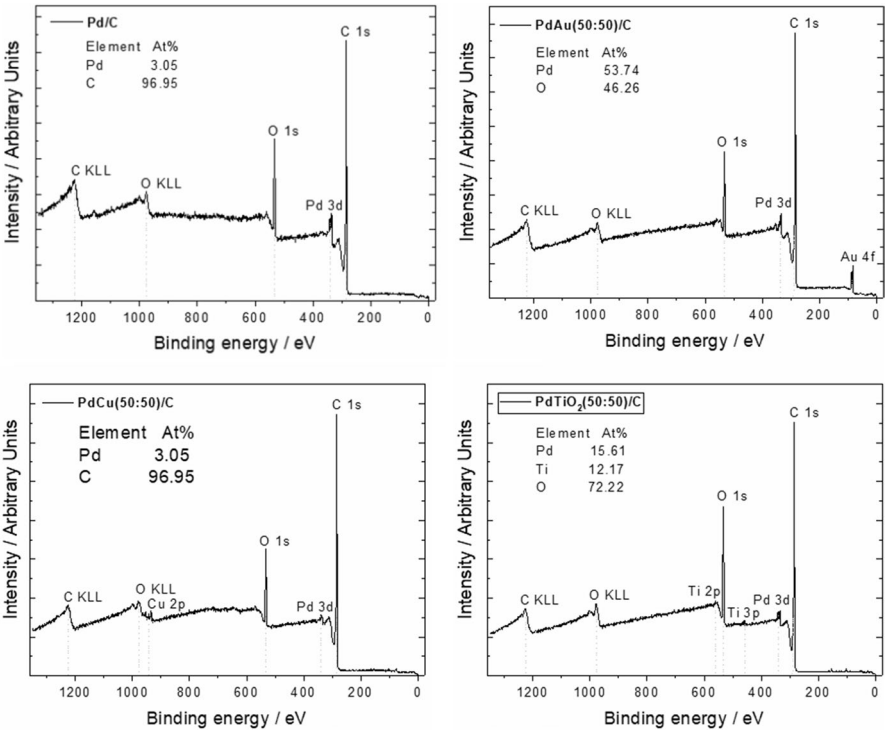

Fig. 3 XPS survey scans of electrocatalyst in full spectrum with the ratio of surface metals

and Pd^{2+}, and the shift was more intense for $PdTiO_2$(50:50)/C [35, 36]. In all electrocatalysts, there is the presence of the PdO; however, the amount of PdO is higher than that of Pd^0 in the Pd/C and PdCu(50:50)/C electrocatalysts achieving 57 and 67%, respectively.

In the case of PdAu/C, the shift of Pd 3d is possible due to Au and/or eventually an electron transfer occurs from Pd to Au (electron affinity: Au-223 kJ mol^{-1}, Pd-54 kJ mol^{-1}) [37–39]. Besides, in Fig. 5 we can see that the Au 4f peaks of PdAu/C electrocatalyst are shifted to lower BEs compared to the literature reported with 83.9 and 87.7 eV to Au° $4f_{7/2}$ and $4f_{5/2}$, respectively [38, 39]. This suggests that there is strong interaction between Pd and Au, attributable to the electron transfer between Pd and Au, with possible formation of an alloy between Pd and Au, as discussed above in the XRD section. To the PdCu/C and $PdTiO_2$/C electrocatalysts, a positive value indicates the formation of an alloy between Pd and Cu or Pd and TiO_2 [40].

The deconvolution of the Cu $2p_{3/2}$ region in Fig. 5 shows two peaks at 932.2 and 934.2 eV corresponding to Cu^{+2} and Cu^0, respectively. Two more peaks are observed in the $2p_{1/2}$ region corresponding to 951.9 eV related to Cu^0, which is in the PdCu alloy state. Another peak at 953.9 eV can be assigned to Cu^{2+} [40–43]. The existence of Cu^{2+} could be attributed to the oxidation of PdCu. The BE of the Ti $2p_{3/2}$ and Ti $2p_{1/2}$ spin orbit doublet at 495.5 and 465.2 are characteristic of the

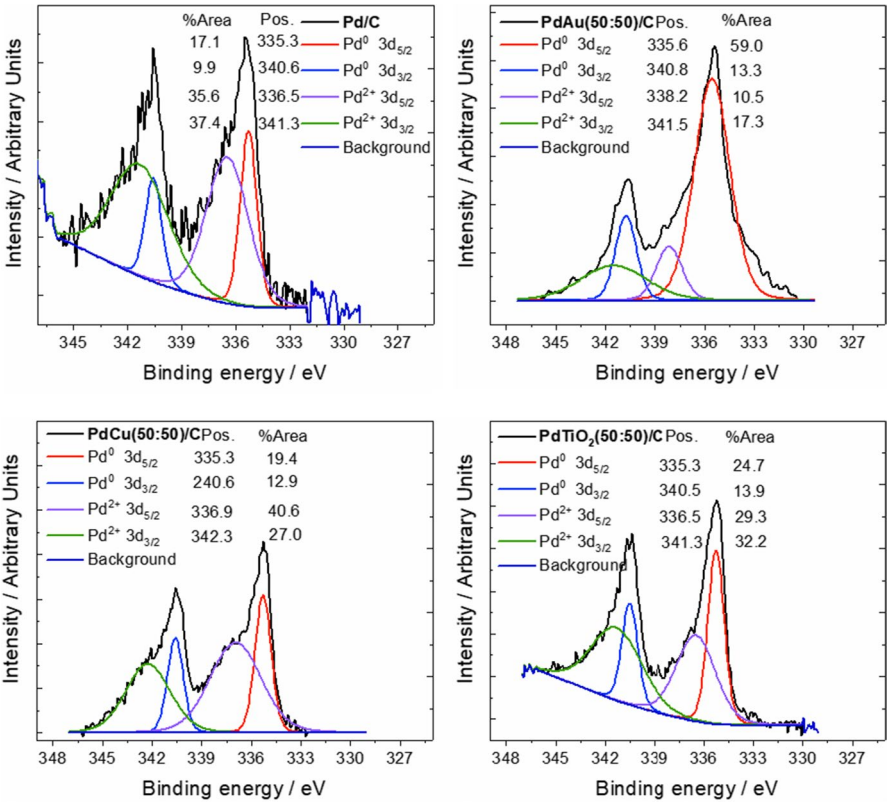

Fig. 4 High-resolution spectra detailing the Pd $3d_{5/2}$ and Pd $3d_{3/2}$ to Pd/C, $PdTiO_2$(50:50)/C, PdAu(50:50)/C and PdCu(50:50)/C electrocatalysts

Ti^{+4} and TiO_2 anatase phase (Fig. 5) [44–45]. No other oxidation degree is detected in this electrocatalyst.

In Fig. 6, are shown the cyclic voltammograms of the Pd/C, PdAu/C, PdCu/C and, $PdTiO_2$/C electrocatalysts, in the presence of 0.5 mol L^{-1} H_2SO_4 saturated with N_2 and ($H_2SO_4 + CH_4$). The CV of Pd/C, PdCu/C, and $PdTiO_2$/C showed a region of adsorption/desorption of hydrogen in the range of 0.05 to 0.4 V versus RHE well defined, while PdAu(50:50)/C electrocatalyst showed a region poorly defined, whose effect could be due to the partial coverage of palladium surface by gold atoms (Au). For all electrocatalysts prepared, in anodic scan some processes of oxidation were observed. These processes could be associated with the formation of oxides or a larger quantity of adsorbed oxygenated species. For PdCu(50:50)/C, a peak at approximately 0.6 V versus RHE was observed, indicating the formation of Cu oxide (Fig. 6c). For Pd/C, PdAu/C, PdCu/C and $PdTiO_2$/C electrocatalysts, the oxidation process between approximately 0.7 to 1.2 V versus RHE is attributed to the formation of palladium oxides. The cathode peaks around 0.7 V versus RHE are attributed to the reduction of palladium oxides formed during negative scanning.

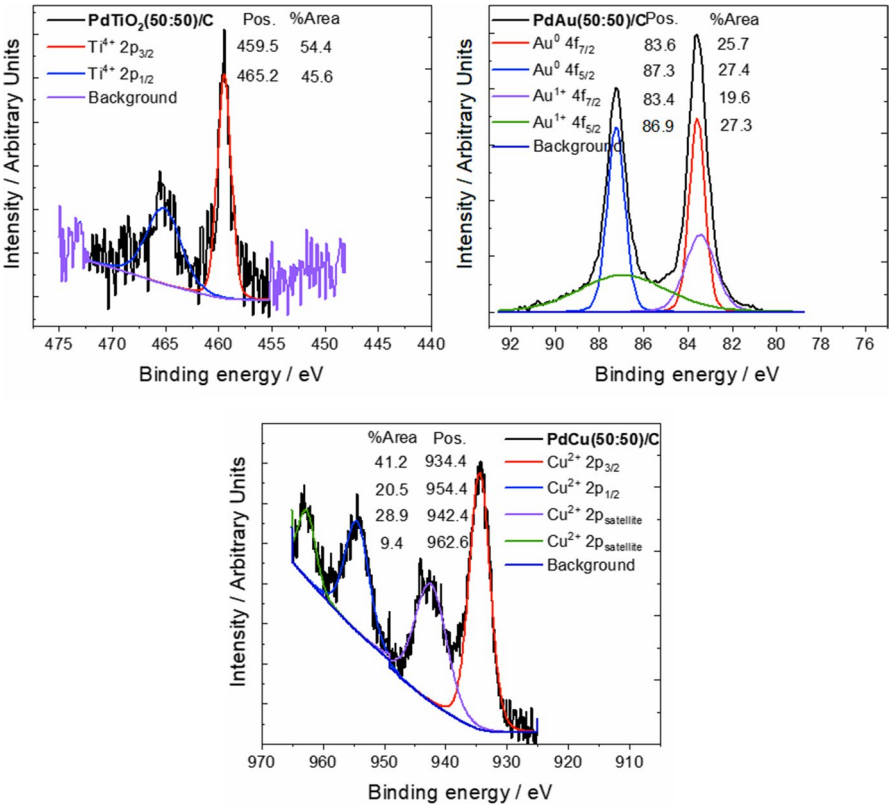

Fig. 5 High-resolution spectra detailing the Ti $2p_{3/2}$ and Ti $2p_{1/2}$ to $PdTiO_2$(50:50)/C. High-resolution spectra detailing the Au $4f_{7/2}$ and Au $4f_{5/2}$ to PdAu(50:50)/C. High-resolution spectra detailing the Cu $2p_{3/2}$ and Cu $2p_{1/2}$ to PdCu(50:50)/C. Sum of the fitting components is provided in brown

The cyclic voltammograms for methane oxidation on the Pd/C, PdAu/C, PdCu/C, and $PdTiO_2$/C electrocatalysts obtained at room temperature, in solution of H_2SO_4 with bubbling of methane gas for 1800 s, under rotation of 900 rpm in a disk rotator (10 mV s^{-1}) are shown in Fig. 6 (curves: black, red, green, and blue).

PdAu/C, PdCu/C, and $PdTiO_2$/C showed that the hydrogen adsorption–desorption region (0.05–0.5 V vs RHE) increased due to adsorption of methane. In the anodic scan, an increase was also observed in current, which corresponds to electrochemical oxidation of the adsorbed species. This result indicated adsorption of hydrogen in the electrode surface, and this process was more pronounced for PdCu/C. However, complementary information about the products from methane oxidation could be obtained by ATR-FTIR measurements, which were also presented in this work.

Figure 7 shows the FTIR spectra in the range of 1200–850 cm^{-1}, a region of the main products of methane electrochemical oxidation on Pd/C, PdAu/C, PdCu/C, and $PdTiO_2$/C electrocatalysts.

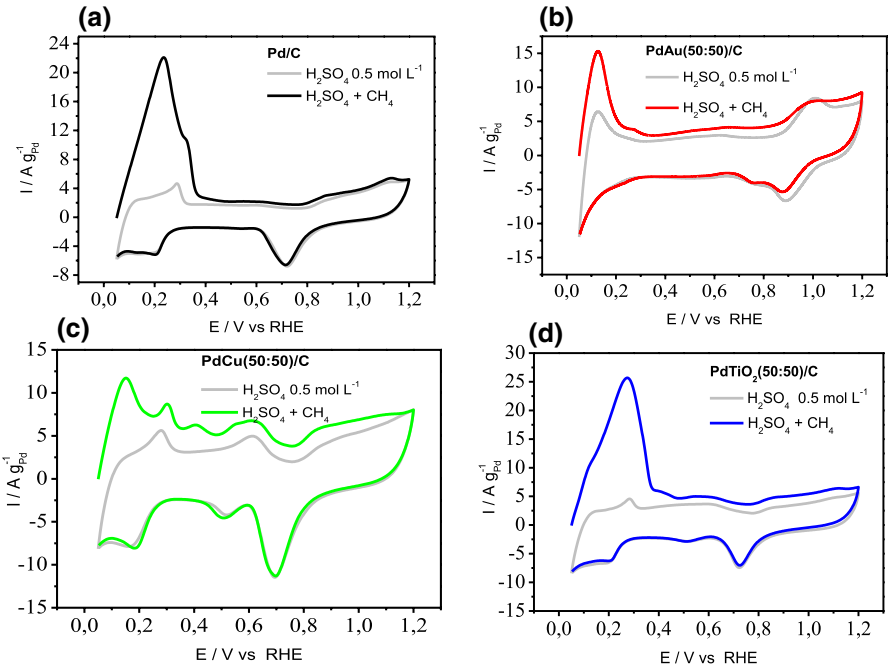

Fig. 6 Cyclic voltammograms of the Pd/C, PdAu(50:50)/C, PdCu(50:50)/C and $PdTiO_2$(50:50)/C electrocatalysts using H_2SO_4 0.5 mol L^{-1} electrolyte saturated with N_2 and those of methane oxidation (H_2SO_4 0.5 mol L^{-1} + CH_4)

For Pd/C, a band was observed at 1078 cm^{-1} from 0.3 V corresponding to CH_3 rock [42]; this band increased at 0.4 V and decreased up to 1.0 V. Another band was observed in 1105 cm^{-1} corresponding to formic acid [46] which appeared in 0.7 V and increased with potential. The band at 1034 cm^{-1} can be corresponding to both C–O str of methanol [46] and CH bend of formic acid [47]. In spectra obtained on PdAu/C, the methanol band (1080 cm^{-1}) appeared in 0.2 V and disappeared close to 0.6 V. The band at 1034 cm^{-1} was shifted to 1045 cm^{-1} with the increase in potential and disappeared at 0.7 V, indicating that methanol and formic acid were totally oxidized. A band at about 1000 cm^{-1} corresponds to ν(COC) in oligomers of the formaldehyde in aqueous solution [48], and it was observed an increase in potential at 0.3 V, and in 0.7 V it was extinct.

In the presence of a Pd (II) with Au(III), methane was converted to the methanol with a yield above 70% at 81% selectivity [49, 50]. This electrocatalyst could promote the functionalization of C-H bonds (Eq. 1) [49–51]:

$$CH_4 + 2H_2SO_4 \xrightarrow{[Pd^{II}],H_2SO_4} CH_3OSO_3H + SO_2 + 2H_2O. \quad (1)$$

The methyl bisulfate can be subsequently hydrolyzed to form methanol (Eq. 2):

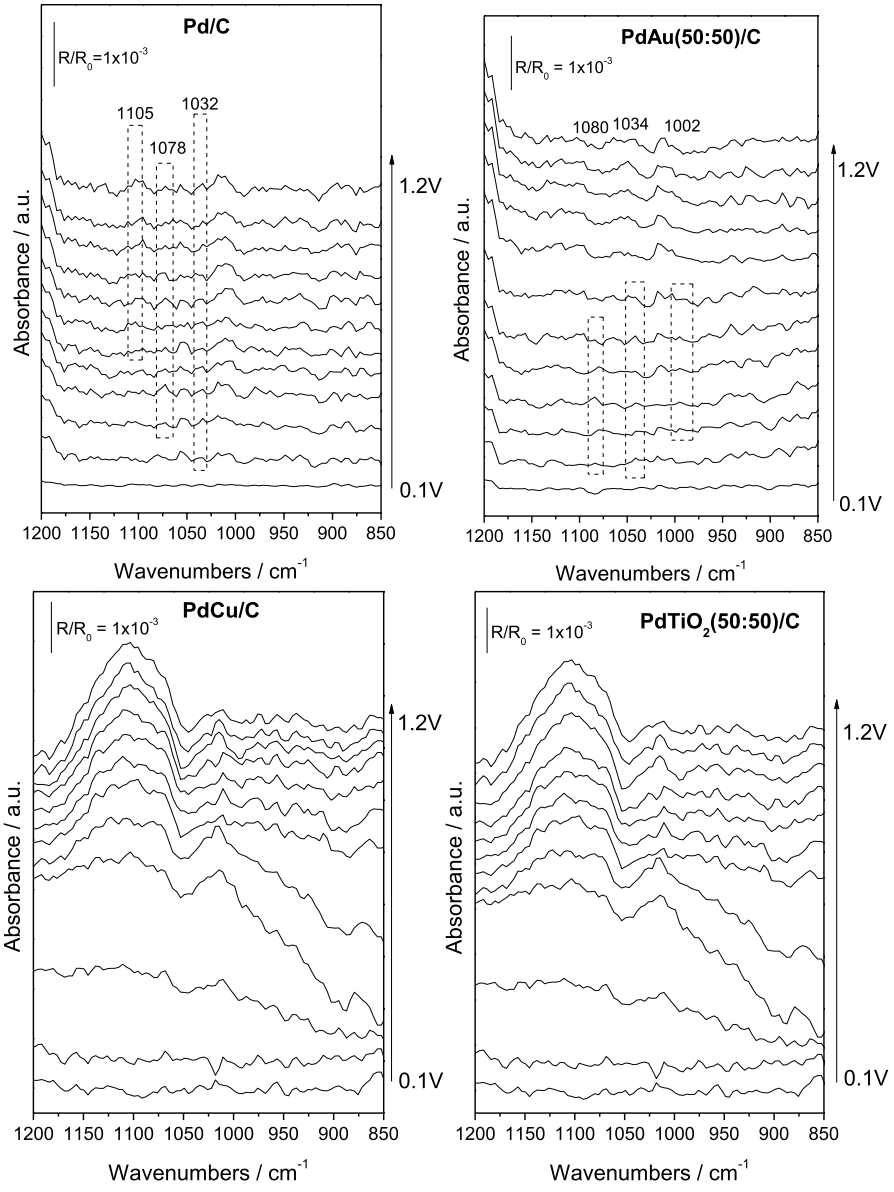

Fig. 7 In situ ATR-FTIR spectra in the range of 1200–850 cm^{-1} of methane (CH_4) oxidation on Pd/C, PdAu(50:50)/C, PdCu(50:50)/C and $PdTiO_2$(50:50)/C electrocatalysts at potentials ranging from 0.05 to 1.2 V with an interval of 0.1 V

$$CH_3OSO_3H + H_2O \rightarrow CH_3OH + SO_2 + \frac{1}{2}O_2 + H_2O. \quad (2)$$

Using H_2SO_4 as a solvent, it is difficult to separate methanol from the solvent; consequently, it is necessary to use materials, and regeneration to spent H_2SO_4 also proves it difficult. Besides, Pd has been used as an electrocatalyst for the oxidation of methane to methanol products in the acid medium [49, 50]. The CH_4 oxidation to H_2O_2 offers considerable advantages over the H_2 oxidation to H_2O_2 because valuable organic oxygenates (methanol and formic acid) can be effectively produced at the same time (Eqs. 3 and 4) [52–54]:

$$CH_{4(g)} + H_2O_{(g)} \rightleftarrows CO_{(g)} + 3H_{2(g)} \Delta H_r^o(298\ \mathrm{K}) = +\ 206\ \mathrm{kJ\ mol^{-1}}\left(CH_4\right) \quad (3)$$

$$H_2 + O_2 \overset{[Pd^{II},Au^{III}]}{\Leftrightarrow} H_2O_2 \longrightarrow CH_4HCOOH, CH_3OH. \quad (4)$$

In the case of formaldehyde production, firstly, CH_4 reacts with O_2 and producesHCHO and H_2O (Eq. 5) [55, 56]:

$$CH_4 + O_2 \rightarrow HCHO + H_2O. \quad (5)$$

Then, the intermediate product HCHO further reacts with O_2 and producesCO_2 and H_2O (Eq. 6):

$$HCHO + O_2 \rightarrow CO_2 + H_2O. \quad (6)$$

The intermediate product formaldehyde can conveniently be oxidized to CO_2 and H_2O in a similar manner, with the involvement of active oxygen species O_2^-, OH^- and O^- [55].

For materials containing non-noble metals (Cu and Ti), a different behavior was observed compared with Pd and PdAu in the bands at 1100 cm^{-1} and 1015 cm^{-1}; this increase in signal can be corresponding to the production of formic acid with attraction of the electrolyte due to the electric field and/or to Cu oxide dissolved [57] and Ti compounds solution [58]; due to the enlargement of this band, it was difficult to observe the methanol bands. However, the partial methane oxidation cannot be discarded due to current peaks observed in the voltammetry experiments with methane nearby 0.4 and 0.5 V, distant of the profiles observed in the cyclic voltammetry without the presence of methane [59].

Figure 8 illustrates the results in a type PEMFC fuel cell using Pd/C, PdAu/C, PdCu/C, and $PdTiO_2$/C as anodic electrocatalysts using Nafion® 117 as a membrane at 80 °C and 150 mL min^{-1} of methane (CH_4).

The PdAu/C and $PdTiO_2$/C electrocatalysts showed an open circuit potential values of 397.70 mV and 355.59 mV, while Pd/C and PdCu/C electrocatalysts were approximately 242.56 mV and 292.35 mV, respectively, (Fig. 8a). The PdAu(50:50)/C electrocatalyst presented a higher value of maximum power density for methane oxidation (0.96 mW cm^{-2} in 3.83 mA cm^{-2}) compared to the $PdTiO_2$(50:50)/C (0.85 mW cm^{-2} in 3.51 mA cm^{-2}), Pd/C (0.50 mW cm^{-2} in 3.95 mA cm^{-2}) and PdCu(50:50)/C (0.57 mW cm^{-2} in 3.51 mA cm^{-2}), indicating the positive effect of cocatalysts added to the Pd for the methane oxidation.

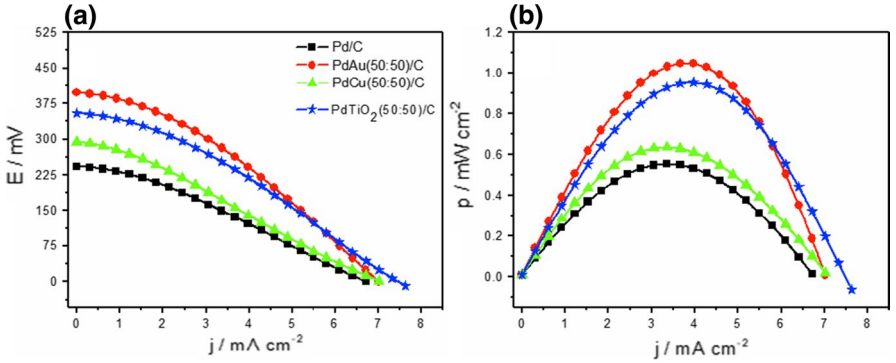

Fig. 8 **a** Polarization and **b** power density curves of a 5-cm^2 direct methane fuel cell using 20 wt% PdAu, PdCu and $PdTiO_2$ materials in the anode and Pt/C at the cathode (1 mg Pt cm^{-2}) and Nafion® 117 as a membrane at 80 °C, using 150 mL min^{-1} of methane (CH_4)

Experiments in single direct methane fuel cells (DMEFC) at 80 °C also revealed that the PdAu(50:50)/C, PdCu/C, and $PdTiO_2$/C electrocatalysts could promote the activity for the methane oxidation in comparison with Pd/C. The presence of Au, Cu or, TiO_2 increased the formation of oxygenated species, which have the function of promoting the oxidation of adsorbed intermediates on the palladium surface (Fig. 8b).

The high electrocatalytic activity of the PdAu(50:50)/C electrocatalyst synthesized by the sodium borohydride reduction process could be attributed to the bifunctional mechanism and to the electronic effect.

Conclusions

The method utilized in this work was an efficient methodology to produce Pd/C, PdAu/C, PdCu/C, and $PdTiO_2$/C for methane oxidation because ICP-MS results showed that the amount of Pd in the synthesized electrocatalysts is close to that expected.

XRD of all electrocatalysts showed a face-centered cubic structure of palladium, and that of $PdTiO_2$/C also showed peaks associated with the tetragonal structure characteristics of titanium oxide anatase phase. TEM images revealed that the nanoparticles were well dispersed in the support; however, the presence of agglomerates and a mean nanoparticle size of 6.9 nm at 8.9 nm were also observed. XPS analysis showed the presence of alloys for PdAu/C and PdCu/C binary electrocatalysts prepared and the presence of Cu and Ti oxides species.

For all the prepared electrocatalysts, in the anodic scan an increase in current was observed in the hydrogen desorption region that doesn't correspond to product formation potentials. However, in the anodic scan, a process of oxidation was also observed that could be attributed to methane oxidation for other products as observed by ATR-FTIR in situ experiments.

The experiments at 80 °C in DMEFC showed that the addition of Au, Cu, and TiO_2 to the Pd/C electrocatalyst promotes the methane activation by the bifunctional mechanism and electronic effect.

However, new studies yet are necessary to investigate the mechanisms of methane activation in alkaline electrolytes using PdAu/C, PdCu)/C, and $PdTiO_2$/C prepared in different atomic compositions.

Acknowledgements The authors thank the CAPES, FAPESP (2014/09087-4, 2014/50279-4, 2017/11937-4, 2017/21846-6 and 2017/22976-0), CINE-SHELL (ANP)/FAPESP Grants (2017/11937-4), and CNPq (300816/2016-2 and 429727/2018-6) for the financial support.

References

1. R. Abbasi, G. Huang, G.M. Istratescu, L. Wu, R.E. Hayes, Can. J. Chem. Eng. **93**(8), 1474 (2015)
2. R.E. Hayes, S.T. Kolaczkowski, *Introduction to catalytic combustion* (Gordon and Breach Science Publishers, Reading, 1997)
3. R.E. Hayes, S.T. Kolaczkowski, P.K.C. Li, S. Awdry, Chem. Eng. Sci. **56**(16), 4815 (2001)
4. N. Radenahmad, A. Afif, P.I. Petra, S.M.H. Rahman, S.-G. Eriksson, A.K. Azad, Renew. Sustain. Energy Rev. **57**, 1347 (2016)
5. B.C.H. Steele, A. Heinzel, Nature **414**, 345 (2001)
6. B. Suleiman, A.S. Abdulkareem, U. Musa, I.A. Mohammed, M.A. Olutoye, Y.I. Abdullahi, Energy Convers. Manag. **117**, 228 (2016)
7. Y. Liu, L. Hua, J. Power Sources **195**(11), 3529 (2010)
8. S. Mekhilef, R. Saidur, A. Safari, Renew. Sustain. Energy Rev. **16**(1), 981 (2012)
9. M. Joglekar, V. Nguyen, S. Pylypenko, C. Ngo, Q. Li, M.E. O'Reilly, T.S. Gray, W.A. Hubbard, T.B. Gunnoe, A.M. Herring, A.B.G. Trewyn, J. Am. Chem. Soc. **138**(1), 116 (2016)
10. A. Maione, F. André, P. Ruiz, Appl. Catal. B Environ. **75**(1–2), 59 (2007)
11. L. Lv, D. Zha, Y. Ruan, Z. Li, X. Ao, J. Zheng, J. Jiang, H.M. Chen, W.-H. Chiang, J. Chen, C. Wang, ACS Nano **12**, 3042 (2018)
12. W.R. Schwartz, L.D. Pfefferle, J. Am. Chem. Soc. **116**(15), 8571 (2012)
13. K. Sekizawa, H. Widjaja, S. Maeda, Y. Ozawa, K. Eguchi, Catal. Today **59**(1–2), 69 (2000)
14. K. Sekizawa, H. Widjaja, S. Maeda, Y. Ozawa, K. Eguchi, Appl. Catal. A Gen **200**(1–2), 211 (2000)
15. P.J. Kulesza, I.S. Pieta, I.A. Rutkowska, A. Wadas, D. Marks, K. Klak, L. Stobinski, J.A. Cox, Electrochim. Acta **110**, 474 (2013)
16. A.O. Neto, J. Nandenha, R.F.B. De Souza, G.S. Buzzo, J.C.M. Silva, E.V. Spinacé, M.H.M.T. Assumpção, J. Fuel Chem. Technol. **42**(7), 851 (2014)
17. X. Chang, T. Wang, Z.-J. Zhao, P. Yang, J. Greeley, R. Mu, G. Zhang, Z. Gong, Z. Luo, J. Chen, Y. Cui, G.A. Ozin, J. Gong, Angew. Chem. Int. Ed. **57**, 15415 (2018)
18. F. Munoz, C. Hua, T. Kwong, L. Tran, T.Q. Nguyen, J.L. Haan, Appl. Catal. B Environ. **174**, 323 (2015)
19. J.C.M. Silva, G.S. Buzzo, R.F.B. de Souza, E.V. Spinacé, A.O. Neto, M.H.M.T. Assumpção, Electrocatalysis **6**, 86 (2015)
20. S.G. da Silva, J.C.M. Silva, G.S. Buzzo, E.V. Spinacé, A.O. Neto, M.H.M.T. Assumpção, Electrocatalysis **6**, 442 (2015)
21. N. Agarwal, S.J. Freakley, R.U. McVicker, S.M. Althahban, N. Dimitratos, Q. He, D.J. Morgan, R.L. Jenkins, D.J. Willock, S.H. Taylor, C.J. Kiely, G.J. Hutchings, Science **358**, 223 (2017)
22. R.M. Piasentin, R.F.B. de Souza, J.C.M. Silva, E.V. Spinacé, M.C. Santos, A.O. Neto, Int. J. Electrochem. Sci. **8**, 435 (2013)
23. A.O. Neto, M. Brandalise, R.R. Dias, J.M.S. Ayoub, A.C. Silva, J.C. Penteado, M. Linardi, E.V. Spinacé, Int. J. Hydrogen Energy **35**(17), 9177 (2010)
24. J. Nandenha, R.F.B. de Souza, M.H.M.T. Assumpção, E.V. Spinacé, A.O. Neto, Int. J. Electrochem. Sci. **8**, 9171 (2013)
25. M. Brandalise, M.M. Tusi, R.M. Piasentin, M.C. dos Santos, E.V. Spinacé, A.O. Neto, Int. J. Electrochem. Sci. **7**, 9609 (2012)

26. J. Nandenha, R.F.B. de Souza, M.H.M.T. Assumpção, E.V. Spinacé, A.O. Neto, Ionics **19**, 1207 (2013)
27. J. Nandenha, E.H. Fontes, R.M. Piasentin, F.C. Fonseca, A.O. Neto, J. Fuel Chem. Technol. **46**(9), 1137 (2018)
28. M.C.L. Santos, J. Nandenha, J.M.S. Ayoub, M.H.M.T. Assumpção, A.O. Neto, J Fuel Chem. Technol **46**(12), 1462 (2018)
29. C.V. Pereira, E.H. Fontes, J. Nandenha, M.H.M.T. Assumpção, A.O. Neto, Int. J. Electrochem. Sci. **13**, 10587 (2018)
30. E.V. Spinacé, R.R. Dias, M. Brandalise, M. Linardi, A.O. Neto, Ionics **16**, 91 (2010)
31. M.H.M.T. Assumpção, J. Nandenha, G.S. Buzzo, J.C.M. Silva, E.V. Spinacé, A.O. Neto, R.F.B. de Souza, J. Power Sources **253**, 392 (2014)
32. C.A. Ottoni, C.E.D. Ramos, R.F.B. de Souza, S.G. da Silva, E.V. Spinacé, A.O. Neto, Int. J. Electrochem. Sci. **13**, 1893 (2018)
33. L. Feng, S. Yao, X. Zhao, L. Yan, C. Liu, W. Xing, J. Power Sources **197**, 38 (2012)
34. W. Li, X. Zhao, A. Manthiram, J. Mater. Chem. A **2**(10), 3468 (2014)
35. T. Cochell, A. Manthiram, Langmuir **28**(2), 1579 (2012)
36. A. Dutta, J. Datta, Int. J. Hydrogen Energy **38**(19), 7789 (2013)
37. A. Dutta, A. Mondal, P. Broekmann, J. Datta, J. Power Sources **361**, 276 (2017)
38. P. Gobbo, Z. Mossman, A. Nazemi, A. Niaux, M.C. Biesinger, E.R. Gilles, M.S. Workentin, J. Mater. Chem. B **2**, 1764 (2014)
39. Y. Suo, Z. Zhang, J. He, Z. Zhang, G. Hu, Ionics **22**(6), 985 (2016)
40. F. Gao, D.W. Goodman, Chem. Soc. Rev. **41**(24), 8009 (2012)
41. F.P. da Silva, J.L. Fiorio, R.V. Gonçalves, E. Teixeira-Neto, L.M. Rossi, Ind. Eng. Chem. Res. **57**, 16209 (2018)
42. Z. Chen, Y.C. He, J.H. Chen, X.Z. Fu, R. Sun, Y.X. Chen, C.P. Wong, J. Phys. Chem. C **122**(16), 8976 (2018)
43. C. Xu, Y. Liu, J. Wang, H. Geng, H. Qiu, J. Power Sources **199**, 124 (2012)
44. M.C. Biesinger, Surf. Interface Anal. **49**, 1325 (2017)
45. A. Zana, C. Rüdiger, J. Kunze-Liebhäuser, G. Granozzi, N.E. Reeler, T. Vosch, M. Arenz, Electrochim. Acta **139**, 21 (2014)
46. D. Steiner, A. Auer, E. Portenkirchner, J. Kunze-Liebhäuser, J. Electroanal. Chem. **812**, 166 (2018)
47. K. Hamada, H. Morishita, Sci. Bull. Fac. Educ. Nagasaki Univ. **26**, 39 (1975)
48. B.S. Beckingham, N.A. Lynd, D.J. Miller, J. Membr. Sci. **550**, 348 (2018)
49. K.Z. Gaca-Zając, B.R. Smith, A. Nordon, A.J. Fletcher, K. Johnston, J. Sefcik, Vib. Spectrosc. **97**, 44 (2018)
50. P. Tomkins, M. Ranocchiari, J.A. Van Bokhoven, Acc. Chem. Res. **50**, 418 (2017)
51. Z. Zakaria, S.K. Kamarudin, Renew. Sustain. Energy Rev. **65**, 250 (2016)
52. R.A. Periana, D.J. Taube, S. Gamble, H. Taube, T. Satoh, H. Fujii, Science **280**, 560 (1998)
53. R. Horn, R. Schlögl, Catal. Lett. **145**, 23 (2015)
54. J.-S. Min, H. Ishige, M. Misono, N. Mizuno, J. Catal. **198**, 116 (2001)
55. Á. López-Martín, A. Caballero, G. Colón, J. Photochem. Photobiol. A Chem. **349**, 216 (2017)
56. X. Chen, Y. Li, X. Pan, D. Cortie, X. Huang, Z. Yi, Nat. Commun. **7**, 12273 (2016)
57. J. Zhou, Y. Xu, X. Zhou, J. Gong, Y. Yin, H. Zheng, H. Guo, ChemSusChem **4**, 1095 (2011)
58. Y. Gong, M. Zhou, Phys. Chem. Chem. Phys. **11**(39), 8714 (2009)
59. J.W. Kauffman, R.H. Hauge, J.L. Margrave, J. Phys. Chem. **89**(16), 3547 (1985)